Supplementary information

Boosting Dynamic Reconstitution of FeCu–N_4 Sites via Doping of Bimetal Nanoparticles in Oxygen Electrocatalysis

Jing Peng[a,†], Bihua Hu[a,†], Zhitong Li[a], Xiongwei Zhong[a], Zhiwei Lei[a], Xingzhu Wang[a,b,*], Baomin Xu[a,*]

[a] Department of Materials Science and Engineering, Southern University of Science and Technology, Shenzhen 518055, China

[b] Shenzhen Putai Technology Co., Ltd, Shenzhen 518110, China

[†] These authors contributed equally to this work.

[*] Corresponding authors

Emails: wangxz@sustech.edu.cn (X. Wang), xubm@sustech.edu.cn (B. Xu)

1. DFT calculation

Theoretical calculations are performed on the basis of density functional theory (DFT), as implemented in the Vienna ab initio simulation packages (VASP) [1]. For geometric optimizations, we have adopted Perdew-Burke-Ernzerhof [2] functional and projector augmented wave (PAW) scheme [3]. All atomic coordinates are allowed to relax until calculated Hellmann-Feynman forces smaller than 0.03 eV $Å^{-1}$ in geometric optimization. The plane wave expansion is chosen and cutoff at the kinetic energy of 400 eV. The simulated unit cells are constructed periodically, where the vacuum space is specified to be 15 Å. In addition, the Brillouin zones are sampled by a (1×1×1) grid generated with Monkhorst-Pack scheme [4]. Explicit solvation model with a monolayer of water has been considered to calculate the solvation energies. By introducing a hydronium in the solvent, the charge is transferred between the water layer and electrode, resulting in a local electric field, which is employed to consider the electric field effects in experimental measurements.

The free energy (ΔG) calculations of each elementary step are based on the standard hydrogen electrode (SHE), which can be written as: $\Delta G = \Delta E + \Delta E_{ZPE} - T\Delta S - neU$ where ΔE represents the total energy difference, ΔE_{ZPE} and ΔS are the change in the zero-point energy and the entropy. n is the number of electrons transferred during the reaction.

The adsorption energy (ΔE_{*OH}) for ORR is calculated as:

$$\Delta E_{*OH} = E_{substrate+*OH} - E_{substrate} - E_{*OH} \quad (1)$$

The four reaction steps in the $4e^-$ ORR path are listed as follows:

$$* + O_2 + H^+ + e^- \rightarrow *OOH \quad (2)$$

$$*OOH + H^+ + e^- \rightarrow *O + H_2O \quad (3)$$

$$*O + H^+ + e^- \rightarrow *OH \quad (4)$$

$$*OH + H^+ + e^- \rightarrow H_2O + * \quad (5)$$

The calculation formula of d-band center ε_d is as follows:

$$\varepsilon_d = \frac{\int_{-\infty}^{+\infty} \varepsilon\rho(\varepsilon)d\varepsilon}{\int_{-\infty}^{+\infty} \varepsilon d\varepsilon} \quad (6)$$

where $\rho(\varepsilon)$ is the density of states of the d orbitals, and ε is the energy eigen value.

2. *Electron transfer number and H_2O_2 yield*

The linear sweep voltammetry (LSV) curves of catalysts are all obtained at a scan rate of 5 mV s^{-1} with various rotating speed from 400 to 2025 rpm. The electron transfer number for ORR can be calculated according to the following Koutechy-Levich(K-L) equation (7-9):

$$1/J=1/J_L+1/J_K=1/B\omega^{0.5}+1/J_K \quad (7)$$

$$B=0.62nFC_0(D_0)^{2/3}v^{-1/6} \quad (8)$$

$$J_k=nFkC_0 \quad (9)$$

Where J stands for the measured current density, B is calculated from the slope of the K-L plot based on Levich equation. J_K and J_L mean the kinetic- and diffusion-limiting current densities, respectively. n is the transferred electron number, F represents the Faraday constant (F=96485 C mol^{-1}), D_0 means the diffusion coefficient of O_2 in 0.1 M KOH aqueous solution (D_0 =1.93×10^{-5} cm^2 s^{-1}), C_0 stands for the real O_2 bulk concentration in the electrolyte (C_0=1.26×10^{-6} mol cm^{-3}), and v represents the kinetic viscosity of electrolyte (v=0.01 cm^2 s^{-1}).

The rotating ring-disk electrode (RRDE, PINE) consists of Pt ring (inner ring Φ 6.25mm and outer ring Φ 7.92mm) and GC disk (Φ 5.61 mm). For RRDE measurements, the LSV curves of catalysts are all collected at a scan rate of 5 mV s^{-1} with the rotating speed of 1600 rpm and the ring potential at 1.5 V versus RHE. The yield of peroxide percentage and the electron transfer number (n) can also be accurately determined by the following equations 10 and 11, respectively.

$$H_2O_2(\%) = 200 \times I_r/N/ (I_r/N+ I_d) \quad (10)$$

$$n = 4 \times I_d/(I_d + I_r/N) \quad (11)$$

where I_d represents disk current, I_r means ring current, and N stands for the current collection efficiency of Pt ring. N is calculated to be 0.37. For testing the accelerated durability of catalysts, the LSV curves before and after various cycles are collected in the range of 0.3 V to 1.2 V (vs. RHE) at a scan rate of 5 mV s^{-1}.

For oxygen evolution reaction (OER) measurement, the preparation process of catalyst ink is fully consistent with the ORR test. And OER activity of catalysts is measured by three electrodes in 1.0 M KOH with a scan rate of 5 mV s^{-1}.

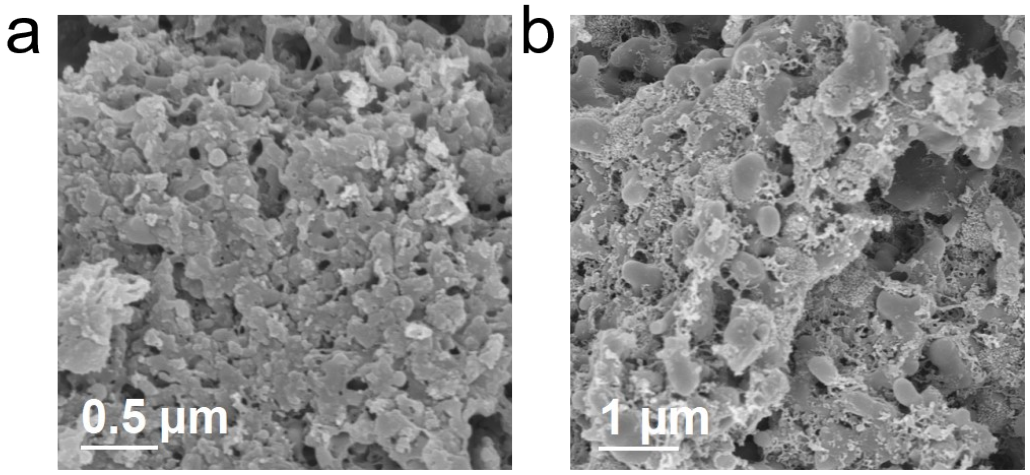

Fig. S1. SEM images of the precursor for (a) $FeCu_{SNP}$@$FeCu_{SA}$/NC and (b) Cu_{SNP}@Cu_{SA}/NC.

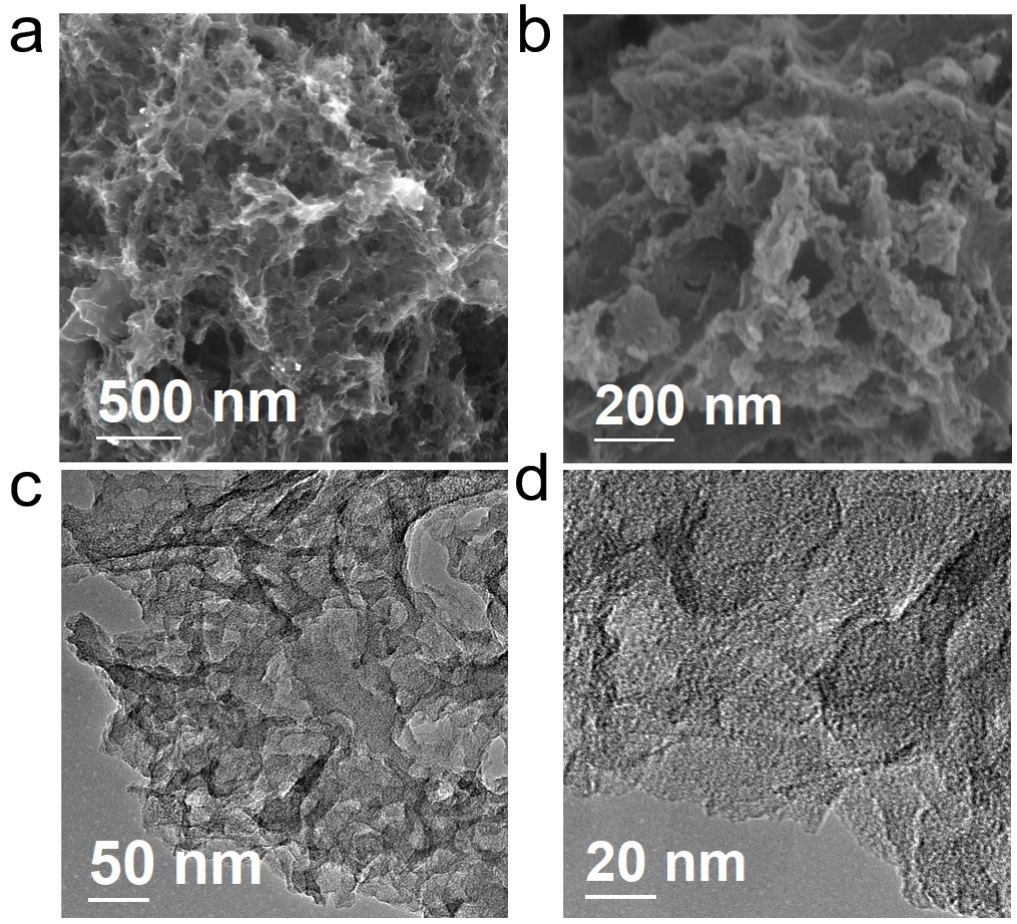

Fig. S2. SEM images of (a) Fe_{SNP}@Fe_{SA}/NC and (b) Cu_{SNP}@Cu_{SA}/NC. (c,d) TEM images of Fe_{SNP}@Fe_{SA}/NC.

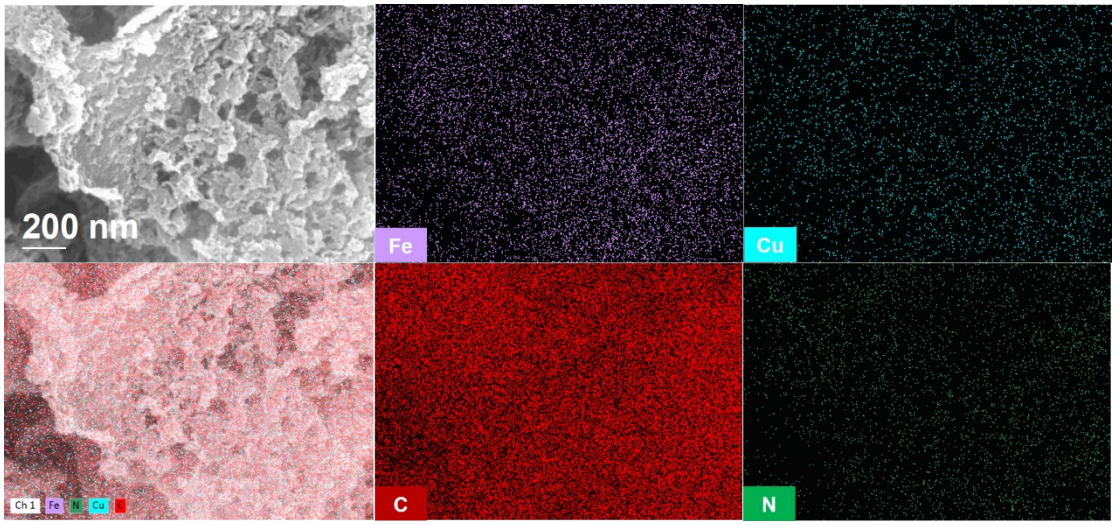

Fig. S3. EDS elemental mappings of the $FeCu_{SNP}$@$FeCu_{SA}$/NC.

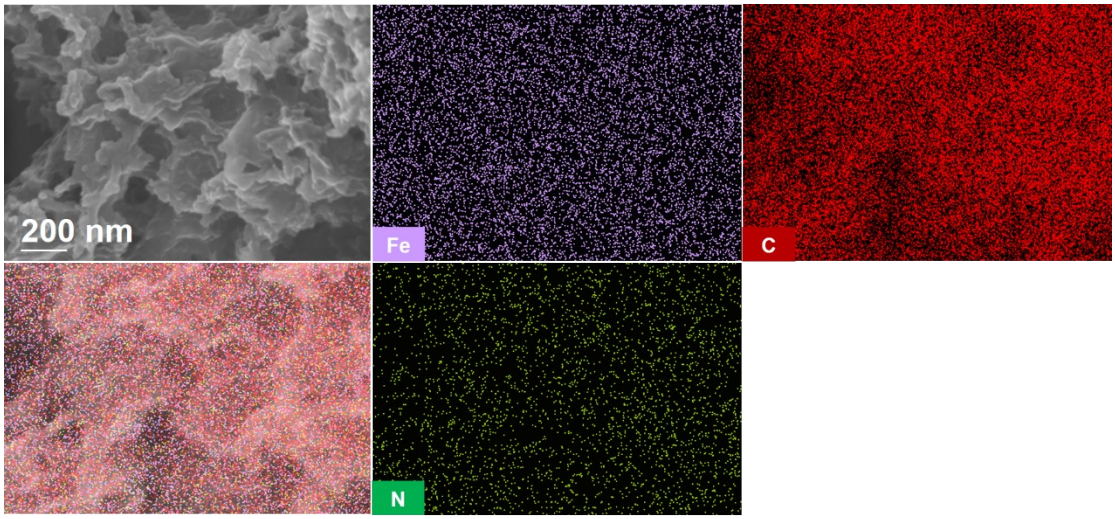

Fig. S4. EDS elemental mappings of the Fe_{SNP}@Fe_{SA}/NC.

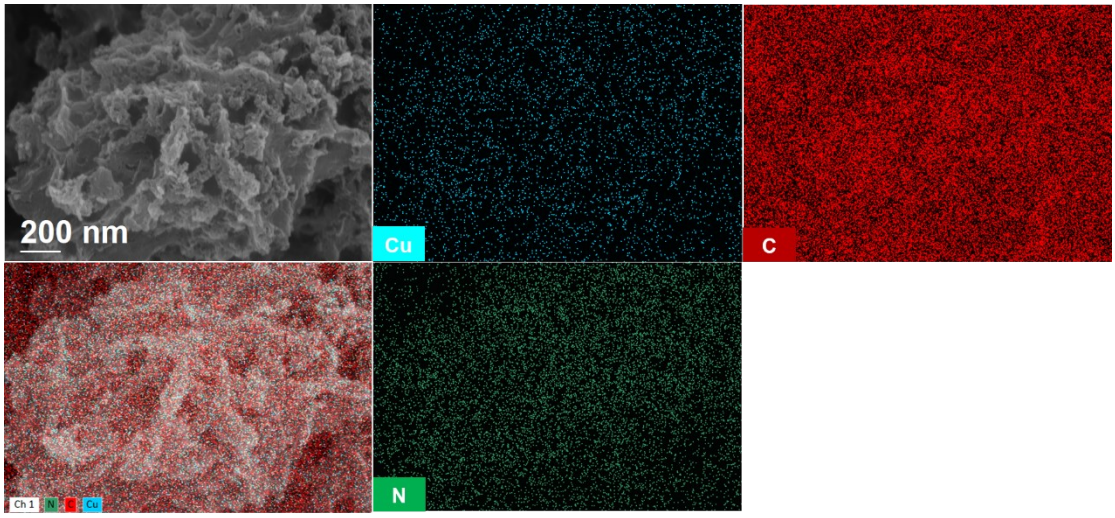

Fig. S5. EDS elemental mappings of the Cu_{SNP}@Cu_{SA}/NC.

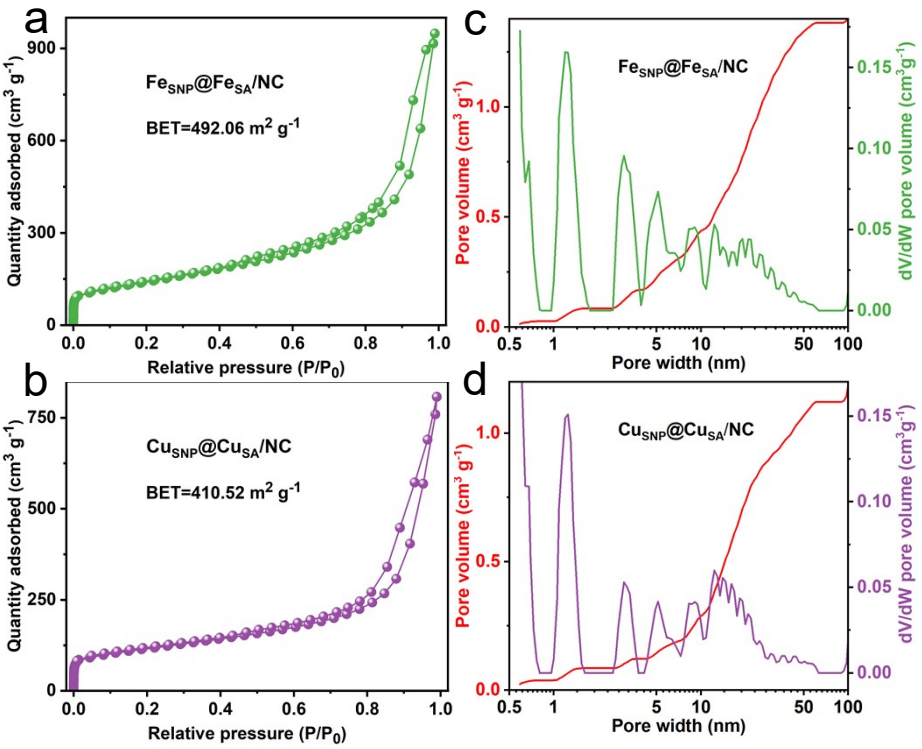

Fig. S6. N_2 adsorption-desorption isotherms of (a) $Fe_{SNP}@Fe_{SA}/NC$ and (b) $Cu_{SNP}@Cu_{SA}/NC$. Distribution of pore width of (c) $Fe_{SNP}@Fe_{SA}/NC$ and (d) $Cu_{SNP}@Cu_{SA}/NC$.

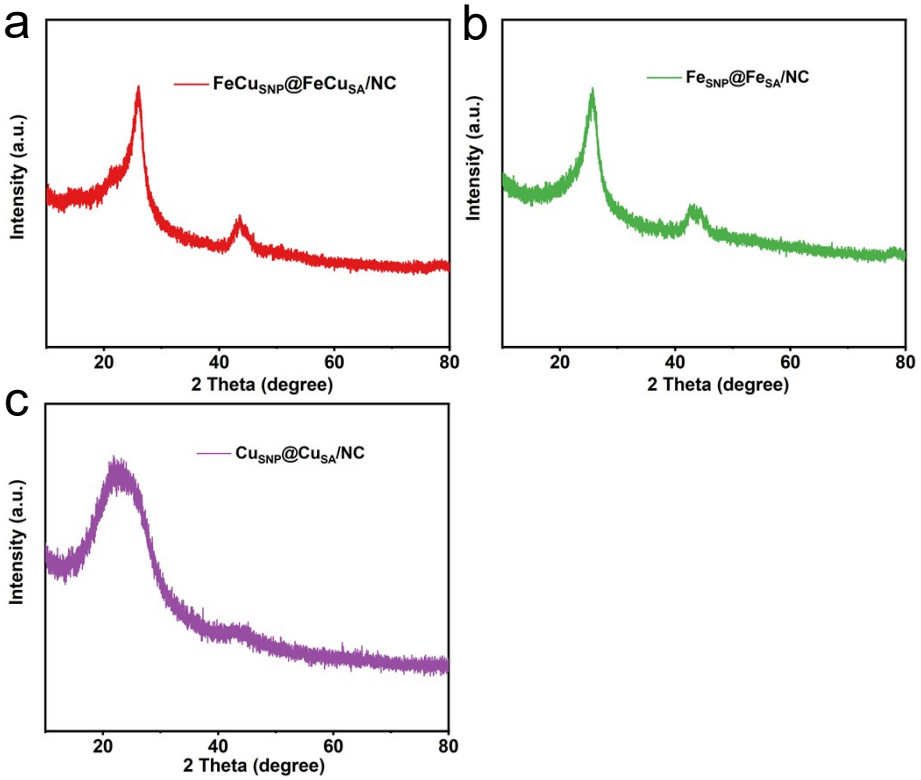

Fig. S7. XRD of (a) $FeCu_{SNP}@FeCu_{SA}/NC$, (b) $Fe_{SNP}@Fe_{SA}/NC$ and (c) $Cu_{SNP}@Cu_{SA}/NC$.

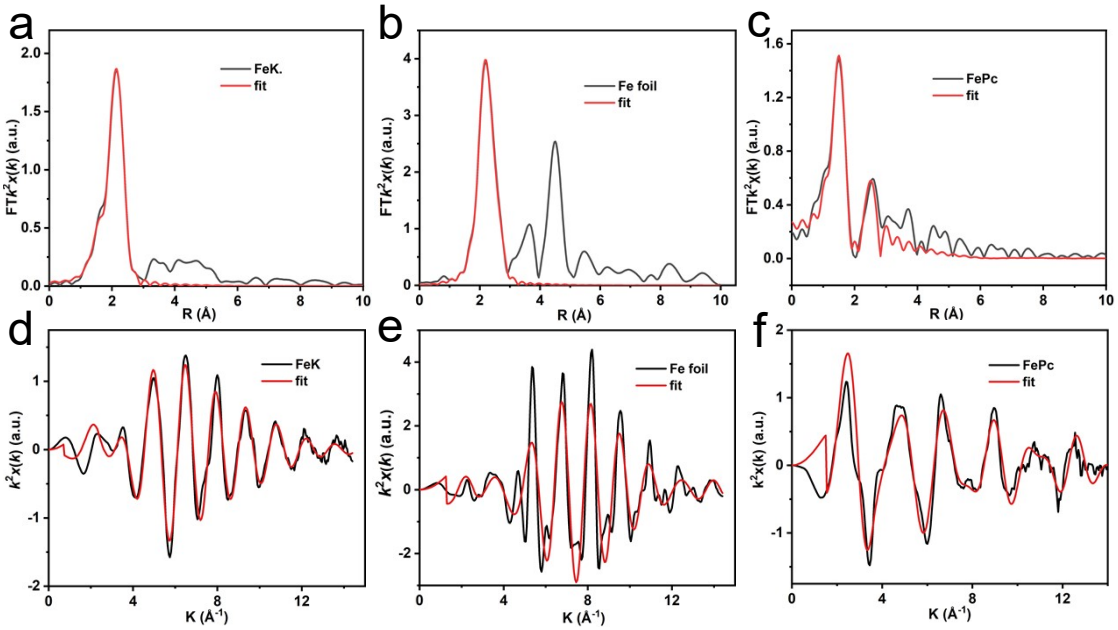

Fig. S8. EXAFS fitting of the Fe R-space curves of (a) $FeCu_{SNP}$@$FeCu_{SA}$/NC, (b) Fe foil and (c) FePc. The corresponding k-space curves and fits of (d) $FeCu_{SNP}$@$FeCu_{SA}$/NC, (e) Fe foil and (f) FePc.

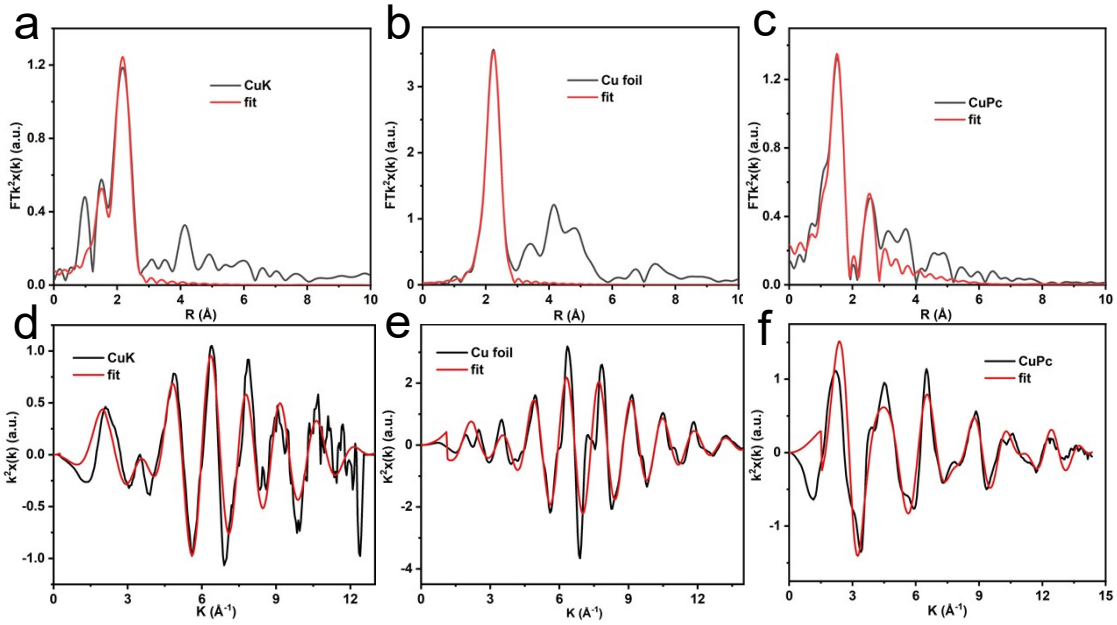

Fig. S9. EXAFS fitting of the Cu R-space curves of (a) $FeCu_{SNP}$@$FeCu_{SA}$/NC, (b) Cu foil and (c) CuPc. The corresponding k-space curves and fits of (d) $FeCu_{SNP}$@$FeCu_{SA}$/NC, (e) Cu foil and (f) CuPc.

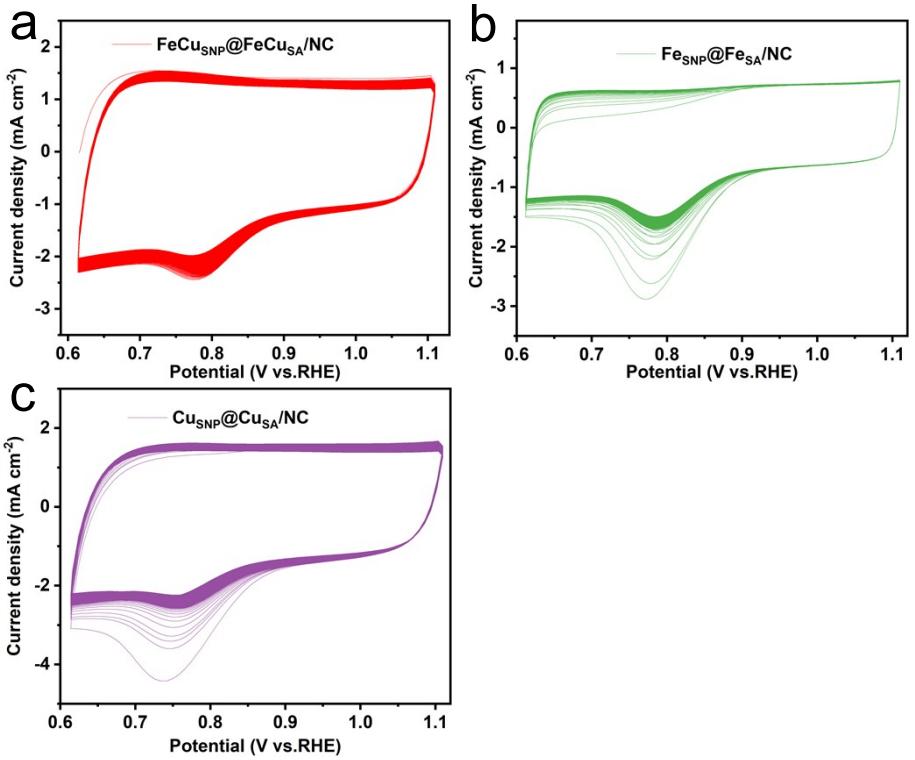

Fig. S10. CV curves of the (a) $FeCu_{SNP}@FeCu_{SA}/NC$, (b) $Fe_{SNP}@Fe_{SA}/NC$ and (c) $Cu_{SNP}@Cu_{SA}/NC$.

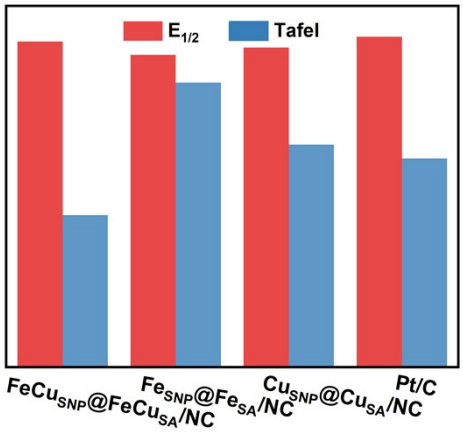

Fig.S11. $E_{1/2}$ and Tafel slopes obtained from the RDE polarization curves for ORR.

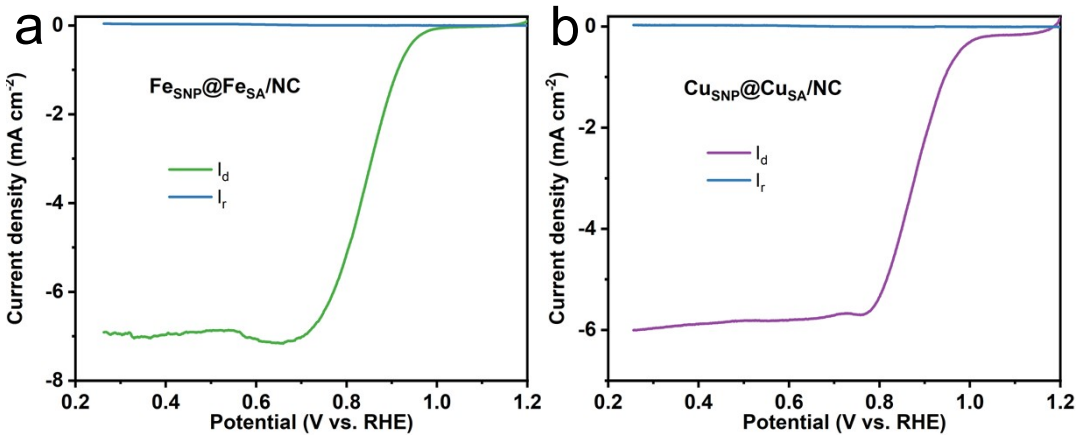

Fig. S12. RRDE measurements of (a) Fe_{SNP}@Fe_{SA}/NC and (b) Cu_{SNP}@Cu_{SA}/NC with a rotation rate of 1600 rpm.

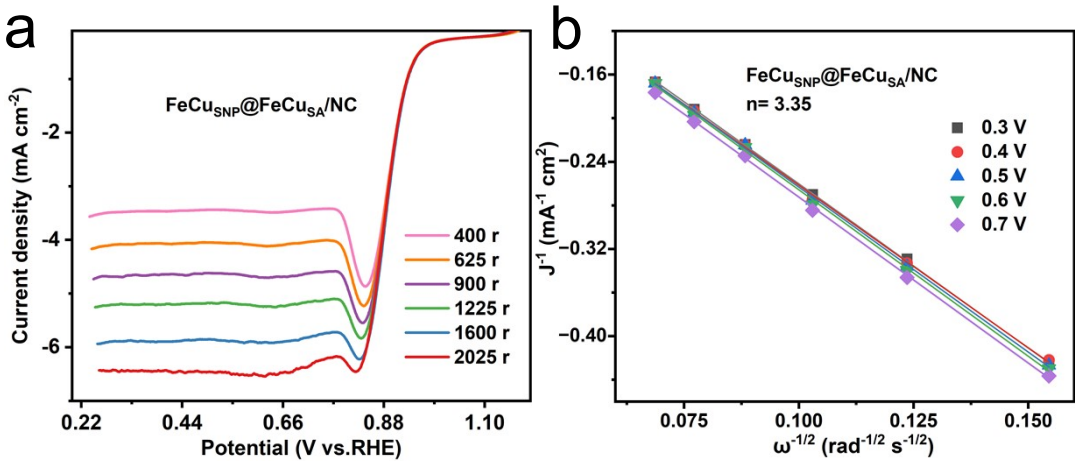

Fig. S13. (a) LSV curves at different rotation rates in rpm of $FeCu_{SNP}$@$FeCu_{SA}$/NC. (b) K-L plots of $FeCu_{SNP}$@$FeCu_{SA}$/NC.

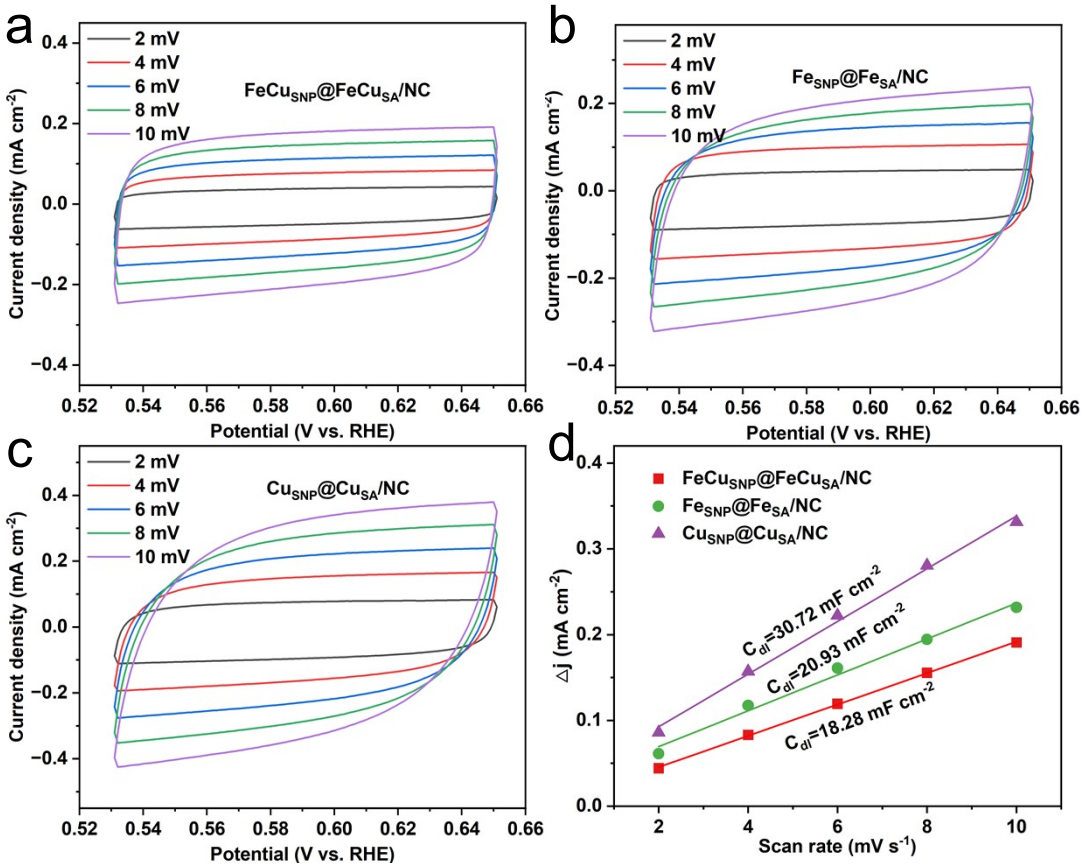

Fig. S14. CV curves for (a) $FeCu_{SNP}$@$FeCu_{SA}$/NC, (b) Fe_{SNP}@Fe_{SA}/NC and (c) Cu_{SNP}@Cu_{SA}/NC at the overpotential window of 0.52-0.66 V versus Hg/HgO, and (d) the calculated ECSA values.

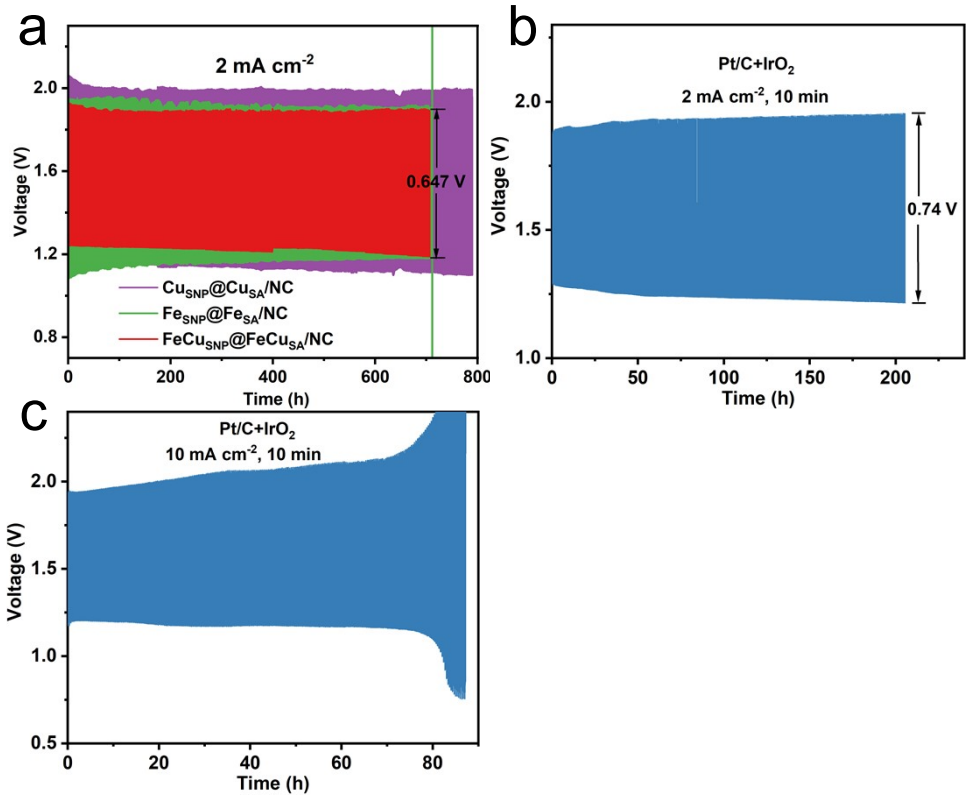

Fig. S15. (a) Long-term cycling performance of $FeCu_{SNP}$@$FeCu_{SA}$/NC, Fe_{SNP}@Fe_{SA}/NC and Cu_{SNP}@Cu_{SA}/NC based ZABs at 2 mA cm^{-2}. Long-term cycling performance of Pt/C+IrO_2 based ZABs at (b) 2 mA cm^{-2} and (c) 10 mA cm^{-2}.

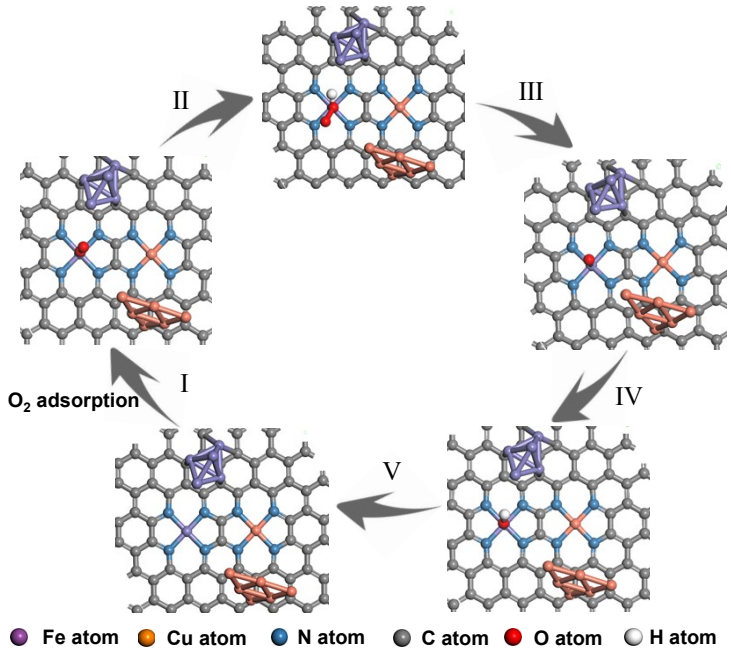

Fig. S16. The ORR pathway based on $FeCu_{SNP}$@$FeCu_{SA}$/NC catalyst.

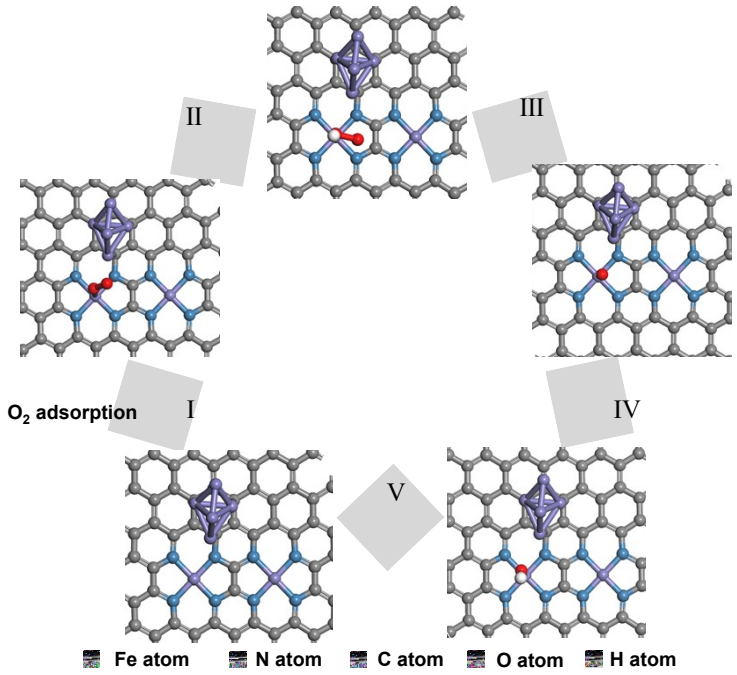

Fig. S17. The ORR pathway based on Fe_{SNP}@Fe_{SA}/NC catalyst.

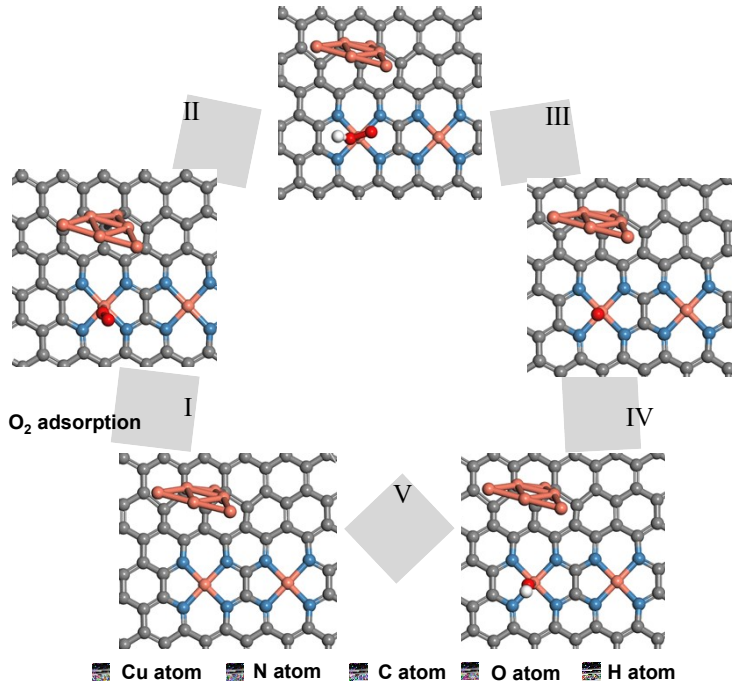

Fig. S18. The ORR pathway based on Cu_{SNP}@Cu_{SA}/NC catalyst.

Table S1 Evaluating the metal atom content in various catalysts by ICP-OES.

Catalysts	Fe atom (%)	Cu atom (%)
$FeCu_{SNP}$@$FeCu_{SA}$/NC	0.2293%	0.3445%
Fe_{SNP}@Fe_{SA}/NC	0.3541%	/
Cu_{SNP}@Cu_{SA}/NC	/	1.196%

Table S2 EXAFS fitting parameters at the Fe K-edge for various samples（S_0^2=0.73）

	shell	CN	R(Å)	σ^2	ΔE_0	R factor
Fe foil	Fe-Fe	8*	2.47±0.01	0.0050	6.2±1.4	0.0066
	Fe-Fe	6*	2.85±0.01	0.0057		
FePc	Fe-N	4.9±0.3	1.93±0.01	0.0015	8.7±1.1	0.0180
	Fe-C	6.7±0.8	2.94±0.01	0.0005		
	Fe-O	6.5±0.6	2.01±0.02	0.0101		
Fe_2O_3	Fe-Fe	4.9±0.5	2.95±0.01	0.0036	1.8±1.4	0.0172
	Fe-Fe1	2.8±0.7	3.74±0.02	0.0008		
FeK.	Fe-N	1.0±0.2	1.89±0.01	0.0041	1.9±0.6	0.0033
	Fe-Fe	6.1±0.1	2.51±0.01	0.0078		

CN: coordination numbers; *R*: bond distance; σ^2: Debye-Waller factors; ΔE_0: the inner potential correction. *R* factor: goodness of fit.

Table S3 EXAFS fitting parameters at the Cu K-edge for various samples (S_0^2=0.84)

	shell	CN	R (Å)	σ^2	ΔE_0	R factor
Cu foil	Cu-Cu	12*	2.54±0.01	0.0085	4.6±0.5	0.0037
	Cu-N	4.3±0.2	1.95±0.01	0.0031		
CuPc					8.7±1.1	0.0134
	Cu-C	4.7±0.6	2.95±0.01	0.0002		
	Cu-O	3.6±0.2	1.95±0.01	0.0062		
CuO					7.0±1.0	0.0122
	Cu-Cu	12.2±1.9	2.97±0.02	0.0260		
	Cu-N	1.0±0.2	1.89±0.02	0.0007		
CuK.					0.2±1.4	0.0170
	Cu-Cu	5.5±0.3	2.50±0.01	0.0104		

CN: coordination numbers; *R*: bond distance; σ^2: Debye-Waller factors; ΔE_0: the inner potential correction. *R* factor: goodness of fit.

Table S4 Comparison of the ORR activity and Tafel slope of $FeCu_{SNP}$@$FeCu_{SA}$/NC and reported cluster/nanoparticle-based catalysts.

Catalysts	**$E_{1/2}$(V)**	**Tafel slope (mV dec^{-1})**	**References**
Fe_{AC}@Fe_{SA}-N-C	0.912	61	R1 [5]
Fe-NPSA@NC	0.72	125	R2 [6]
Fe_{SA}/Fe_{AC}-2DNPC	0.81	54.5	R3 [7]
Fe/Meso-NC-1000	0.885	56	R4 [8]
Co-SAs/SNPs@NC	0.898	65	R5 [9]
Fe/NC-2	0.865	105	R6 [10]
Cu SA/SrGO	0.86	77.1	R7 [11]
Fe SAs/NPs@NC	0.898	59	R8 [12]
Fe_{SA}-Fe_{AC}@NSC	0.90	42.25	R9 [13]
SA-CoCu@Cu/CoNP	0.88	59.9	R10 [14]
Fe(0)@FeNC	0.852	72	R11 [15]
Fe-N-HMCTs	0.841	/	R12 [16]
Co-SAs@NC	0.82	/	R13 [17]
FeCo-NCNT	0.861	/	R14 [18]
$FeCu_{SNP}$@$FeCu_{SA}$/NC	0.883	42.13	This work

Table S5 Comparison of the OER activity between $FeCu_{SNP}$@$FeCu_{SA}$/NC and the corresponding counterparts.

Catalysts	η_{10} E(j=10 mA cm^{-2})
$FeCu_{SNP}$@$FeCu_{SA}$/NC	375.9 mV
Fe_{SNP}@Fe_{SA}/NC	398 mV
Cu_{SNP}@Cu_{SA}/NC	457.6 mV
IrO_2	403 mV

References

1. H. G. Yang, C. H. Sun, S. Z. Qiao, J. Zou, G. Liu, S. C. Smith, H. M. Cheng and G. Q. Lu, *Nature*, 2008, **453**, 638-641.
2. J. Perdew, K. Burke, M. Ernzerhof, *Phy. Review Lett.*, 1996, **77**, 3865-3868..
3. L. Schimka, J. Harl, A. Stroppa, A. Gruneis, M. Marsman, F. Mittendorfer and G. Kresse, *Nat. Mater.*, 2010, **9**, 741-744.
4. H. J. Monkhorst and J. D. Pack, *Phy. Review B*, 1976, **13**, 5188-5192.
5. X. Ao, W. Zhang, Z. Li, J. G. Li, L. Soule, X. Huang, W. H. Chiang, H. M. Chen, C. Wang, M. Liu and X. C. Zeng, *ACS Nano*, 2019, **13**, 11853-11862.
6. H. Huang, D. Yu, F. Hu, S. C. Huang, J. Song, H. Y. Chen, L. L. Li and S. Peng, *Angew. Chem. Int. Ed.*, 2022, **61**, e202116068.
7. X. Wan, Q. Liu, J. Liu, S. Liu, X. Liu, L. Zheng, J. Shang, R. Yu and J. Shui, *Nat. Commun.*, 2022, **13**, 2963.
8. S. N. Zhao, J. K. Li, R. Wang, J. Cai and S. Q. Zang, *Adv. Mater.*, 2022, **34**, e2107291.
9. Z. Wang, C. Zhu, H. Tan, J. Liu, L. Xu, Y. Zhang, Y. Liu, X. Zou, Z. Liu and X. Lu, *Adv. Funct. Mater.*, 2021, **31**, 2104735.
10. M. Liu, J. Lee, T. C. Yang, F. Zheng, J. Zhao, C. M. Yang and L. Y. S. Lee, *Small Methods*, 2021, **5**, e2001165.
11. R. Li, J. Xu, Q. Zhao, X. Yan, J. Ba, Y. Song, R. Zeng, Q. Pan, T. Tang and W. Luo, *Sci. China Mater.* 2022, **66**, 1427-1434.
12. W.-J. Niu, Y.-Y. Yan, R.-J. Li, W.-W. Zhao, J.-L. Chen, M.-J. Liu, B. Gu, W.-W. Liu and Y.-L. Chueh, *Chem. Engin. J.*, 2023, **456**, 140858.
13. W. Zhai, S. Huang, C. Lu, X. Tang, L. Li, B. Huang, T. Hu, K. Yuan, X. Zhuang and Y. Chen, *Small*, 2022, **18**, e2107225.
14. Q. Zhang, P. Kumar, X. Zhu, R. Daiyan, N. M. Bedford, K. H. Wu, Z. Han, T. Zhang, R. Amal and X. Lu, *Adv. Energy Mater.*, 2021, **11**,2100303.
15. X. Cui, L. Gao, S. Lei, S. Liang, J. Zhang, C. D. Sewell, W. Xue, Q. Liu, Z. Lin and Y. Yang, *Adv. Funct. Mater.*, 2020, **31**, 2009197.
16. Z. Li, L. Wei, W.-J. Jiang, Z. Hu, H. Luo, W. Zhao, T. Xu, W. Wu, M. Wu and J.-S. Hu, *Appl. Catal. B: Environ.*, 2019, **251**, 240-246.
17. X. Han, X. Ling, Y. Wang, T. Ma, C. Zhong, W. Hu and Y. Deng, *Angew. Chem. Int. Ed.*, 2019, **58**, 5359-5364.
18. Y. Tan, Y. Wang, A. Li, Y. Zhang, Y. Zhang and C. Cheng, *Mater. Today Energy*, 2022, **29**, 101138.